

## Absorption Spectrum and Solvatochromism of the [Ru(4,4'-COOH-2,2'-bpy)<sub>2</sub>(NCS)<sub>2</sub>] Molecular Dye by Time Dependent Density Functional Theory

Simona Fantacci,<sup>\*,†,‡</sup> Filippo De Angelis,<sup>†,‡</sup> and Annabella Selloni<sup>‡</sup>

Contribution from the Istituto CNR di Scienze e Tecnologie Molecolari (ISTM) c/o Dipartimento di Chimica, Università degli studi di Perugia, via Elce di Sotto, 8, I-60123 Perugia, Italy, and Department of Chemistry, Princeton University, Princeton, New Jersey 08540

Received June 4, 2002; E-mail: simona@thch.unipg.it

**Abstract:** We present a combined Density Functional/Time Dependent Density Functional study of the molecular structure, electronic states, and optical absorption spectrum of [Ru(4,4'-COOH-2,2'-bpy)<sub>2</sub>(NCS)<sub>2</sub>], a widely used charge-transfer sensitizer in nanocrystalline TiO<sub>2</sub> solar cells. Calculations have been performed both for the complex in vacuo and in ethanol and water solvents, using a continuum model to account for solute-solvent interactions. Inclusion of the solvent leads to important changes of the energies and composition of the molecular orbitals of the complex; as a consequence, whereas the computed spectrum for the Ru-complex in vacuo deviates from the experimental one in both energy and shape, the spectra calculated in the presence of the solvent are in good agreement with the experiment. The first two absorption bands are found to originate from mixed ruthenium-NCS to bipyridine- $\pi^*$  transitions rather than to pure metal-to-ligand-charge-transfer (MLCT) transitions, whereas the third band arises from intraligand  $\pi \rightarrow \pi^*$  transitions. The experimentally observed blue-shift of the spectrum in water with respect to ethanol is well reproduced by our calculations and appears to be related to a decreased dipole moment in the excited state.

### I. Introduction

Photoelectrochemical solar cells based on nanostructured TiO<sub>2</sub> electrode have attracted considerable interest over the last 10 years, as they offer the prospect of cheap fabrication, flexibility, and, at the same time, high energy conversion efficiency.<sup>1,2</sup> One of the basic components of these cells is the light-absorbing dye molecule which is used to sensitize the semiconductor electrode. Besides being capable to strongly adsorb onto the semiconductor surface so as to ensure the required electronic coupling for charge injection, an efficient solar cell sensitizer should exhibit intense absorption in the visible part of the spectrum and form long-living excited states with energies matching those of the conduction band of the semiconductor substrate.<sup>1</sup> In the attempt to find dyes satisfying these requirements, hundreds of different molecules have been synthesized and analyzed.<sup>2-4</sup> In this context, the ruthenium-polypyridyl complex *cis*-[Ru(4,4'-COOH-2,2'-bpy)<sub>2</sub>(NCS)<sub>2</sub>] (hereafter referred to as N3), has been identified as a particularly efficient

photosensitizer because of its broad range of visible light absorption, relatively long-lived excited states, and high thermal stability; moreover, the presence of terminal acidic carboxylic groups allows stable anchoring of the dye to the semiconductor surface.<sup>5-11</sup>

The absorption bands in the visible of ruthenium-polypyridyl complexes are usually assigned to metal-to-ligand-charge-transfer (MLCT) transitions,<sup>6</sup> in which an electron is promoted from a Ru-based molecular orbital, belonging to the filled metal  $t_{2g}$  shell, to the empty  $\pi^*$  orbitals of the bipyridine ligands. In particular, the experimental absorption spectrum of the N3 complex in ethanol exhibits two bands in the visible and near-UV regions centered at 538 nm (2.30 eV) and 398 nm (3.12 eV), and a band in the UV region centered at 314 nm (3.95 eV).<sup>6</sup> The first two bands (I and II) are assigned to  $t_{2g} \rightarrow \pi^*$  absorption transitions while the latter (III) is due to the

<sup>†</sup> Istituto CNR di Scienze e Tecnologie Molecolari (ISTM) c/o Dipartimento di Chimica, Università degli studi di Perugia.

<sup>‡</sup> Department of Chemistry, Princeton University.

- (1) Hagfeldt, A.; Grätzel, M. *Acc. Chem. Res.* **2000**, *33*, 269. Grätzel, M. *Nature* **2001**, *414*, 338.
- (2) Kalyanasundaram, K.; Grätzel, M. *Coord. Chem. Rev.* **1998**, *177*, 347.
- (3) Nazeeruddin, Md. K.; Péchy, P.; Renouard, T.; Zakeeruddin, S. M.; Humphry-Baker, R.; Comte, P.; Liska, P.; Cevey, L.; Costa, E.; Shklover, V.; Spiccia, L.; Deacon, G. B.; Bignozzi, C. A.; Grätzel, M. *J. Am. Chem. Soc.* **2001**, *123*, 1613.
- (4) Zakeeruddin, S. M.; Nazeeruddin, Md. K.; Humphry-Baker, R.; Péchy, P.; Quagliotto, P.; Barolo, C.; Viscardi, G.; Grätzel, M. *Langmuir* **2002**, *18*, 952.

- (5) Nazeeruddin, Md. K.; Kay, A.; Rodicio, I.; Humphry-Baker, R.; Müller, E.; Liska, P.; Vlachopoulos, N.; Grätzel, M. *J. Am. Chem. Soc.* **1993**, *115*, 6382.
- (6) Shklover, V.; Nazeeruddin, Md. K.; Zakeeruddin, S. M.; Barbè, C.; Kay, A.; Haibach, T.; Steurer, W.; Hermann, R.; Nissen, H.-U.; Grätzel, M. *Chem. Mater.* **1997**, *9*, 430.
- (7) Shklover, V.; Ovchinnikov, Yu. E.; Graginsky, L. S.; Zakeeruddin, S. M.; Grätzel, M. *Chem. Mater.* **1998**, *10*, 2533.
- (8) Nazeeruddin, Md. K.; Zakeeruddin, S. M.; Humphry-Baker, R.; Gorelsky, S. I.; Lever, A. B. P.; Grätzel, M. *Coord. Chem. Rev.* **2000**, *208*, 213.
- (9) Nazeeruddin, Md. K.; Zakeeruddin, S. M.; Humphry-Baker, R.; Jirousek, M.; Liska, P.; Vlachopoulos, N.; Shklover, V.; Fisher, C.-H.; Grätzel, M. *Inorg. Chem.* **1999**, *38*, 6298.
- (10) Zakeeruddin, S. M.; Nazeeruddin, Md. K.; Humphry-Baker, R.; Grätzel, M. *Inorg. Chim. Acta* **1999**, *296*, 250.
- (11) Amirnasr, M.; Nazeeruddin, Md. K.; Grätzel, M. *Thermochim. Acta* **2000**, *348*, 105.

intraligand  $\pi \rightarrow \pi^*$  transitions of the 4,4'-COOH-2,2'-bispyridine (dcbpy) ligands.<sup>6</sup> In addition, this complex shows a pronounced negative solvatochromism, resulting in a blue-shift of the UV-vis absorption bands in water with respect to ethanol.<sup>6,9</sup> Such solvent-induced shifts are usually interpreted in terms of the different solvation interactions between the polar groups bound to the metal center and the solvent, and mainly depend on solvent polarity and hydrogen-bond.<sup>12</sup> Moreover, a pH dependence of the absorption energies is observed in water, with a red-shift of the three main spectral features with decreasing pH.<sup>9</sup>

Main Features of the Experimental Spectra Are Summarized in the Table below

	I	II	III
C <sub>2</sub> H <sub>5</sub> OH <sup>6,9</sup>	538 (2.30) 13.1	398 (3.12) 13.0	314 (3.95) 49.4
H <sub>2</sub> O <sup>6,9</sup> (pH = 7)	500 (2.48) 13.1	372 (3.33) 12.4	308 (4.03) 49.0
H <sub>2</sub> O <sup>9</sup> (pH = 1) <sup>a</sup>	520 (2.38)	390 (3.18)	312 (3.97)

The three maxima in the absorption spectra of N3 in different solvents. For each entry, the first value is the position of the maximum in nm, the second, in parentheses, is the corresponding value in eV,<sup>13</sup> while the third value is  $\epsilon \times 10^3$  [M<sup>-1</sup> cm<sup>-1</sup>]. <sup>a</sup> The pK<sub>a2</sub>, corresponding to the complete protonation of the four acidic carboxylic groups, is 1.5.<sup>9</sup>

In contrast to the numerous experimental studies, so far only a few theoretical investigations limited to the gas-phase, and generally based on semiempirical approaches, have been performed to study the electronic structure of the N3 complex.<sup>14,15</sup> Only very recently, a Time Dependent Density Functional Theory (TD-DFT) study on the tetra-deprotonated form of the N3 complex limited to the gas-phase has been carried out, but no geometry optimization of the molecular structure was performed.<sup>16</sup> On the other hand, a theoretical investigation was performed at the semiempirical ZINDO level on the analogous [Ru(4,4'-COOH-2,2'-bpy)<sub>2</sub>(Cl)<sub>2</sub>] complex,<sup>8</sup> for which the geometry was optimized using DFT calculations, whereas a complete DFT study has been carried out for the prototype [Ru(bpy)<sub>3</sub>]<sup>2+</sup> complex.<sup>17</sup>

In this paper, we present a fully first principles investigation of the [Ru(4,4'-COOH-2,2'-bpy)<sub>2</sub>(NCS)<sub>2</sub>] complex, including DFT calculations of the structural and electronic properties of both the cis and trans isomers, as well as a TD-DFT<sup>18,19</sup> study of the main features of the near UV-vis spectrum of the cis isomer both in the gas-phase and in two solvents, ethanol, and water. TD-DFT calculations have proven quite reliable in describing the electronic spectra of complexes containing transition metals,<sup>20–22</sup> also in solution.<sup>23</sup> In this work, we show that with a reasonable computational effort TD-DFT well reproduces the spectroscopic properties of the N3 dye, suggest-

ing that this approach could be used to provide insight for the design of new and more efficient solar cells sensitizers.

## II. Method and Computational Details

For our calculations we used the ADF (Amsterdam Density Functional) program package,<sup>24–26</sup> including the time-dependent extension of density functional theory implemented in this code.<sup>27</sup>

The TD-DFT procedure consists of two steps: the SCF step to generate the Kohn–Sham orbitals and relative orbital energies, and a post-SCF step to solve the eigenvalue equation

$$\Omega F_i = \omega_i^2 F_i \quad (1)$$

where the  $\omega_i$  are the single-excitation energies and the oscillator strengths are obtained from the eigenvectors  $F_i$ , which can be used for an approximate description of the excited states.<sup>18</sup> The components of the four-index matrix  $\Omega$  are defined in terms of occupied and virtual orbital energies and of the so-called coupling matrix which contains Coulomb and exchange-correlation (XC) parts.<sup>18</sup> For large molecules, such as the complex considered in this work, eq 1 is solved via an iterative procedure based on the Davidson algorithm.

In this TD-DFT procedure, two approximations are generally made: one for the XC potential, and one for the XC kernel, which is the functional derivative of the time-dependent XC potential with respect to the density. We used the BPW91 gradient corrected functional in the SCF step (including the Vosko-Wilk-Nusair LDA parametrization<sup>28</sup> and Becke<sup>29</sup> and Perdew-Wang<sup>30</sup> gradient corrections to the exchange and correlation, respectively), and the Adiabatic Local Density Approximation (ALDA) for the XC kernel, in the post-SCF step. To test the dependence of our results on the choice of the XC functional, the absorption spectrum of the N3 complex in vacuo was calculated using also the asymptotically correct van Leeuwen–Baerends functional (LB94)<sup>31</sup> in the SCF step. In the LB94 functional, the exchange-correlation potential is computed from the exact charge density, whereas for BPW91 functional a less expensive density fitting procedure is used. We discuss the results of these calculations in Section III.C, see below.

Geometry optimizations were performed using the standard ADF IV basis set<sup>32</sup> for Ru, which is an uncontracted triple-STO basis set, with a triple-nd, ( $n + 1$ )s basis with one ( $n + 1$ )p function, and the ADF III basis set<sup>32</sup> for the remaining atoms, which is an uncontracted double-STO basis set with one 3d polarization function for C, N and

(12) Reichardt, C. *Chem. Rev.* **1994**, *94*, 2319.

(13) Pyykkö, P.; Zhao, Y. Report HUKI 1-89 ISSN 0784-0365 **1989**.

(14) Rensmo, H.; Södergren, S.; Patthey, L.; Westmark, K.; Vayssieres, L.; Khole, O.; Brühwiler, P. A.; Hagfeldt, A.; Siegbahn, H. *Chem. Phys. Lett.* **1997**, *274*, 51.

(15) Cecchet, F.; Gioacchini, A. M.; Maccaccio, M.; Paolucci, F.; Roffia, S.; Alebbi, M.; Bignozzi, C. A. *J. Phys. Chem. B* **2002**, *106*, 3926.

(16) Monat, J. E.; Rodriguez, J. H.; McCusker J. K. *J. Phys. Chem. A* **2002**, *106*, 7399.

(17) Daul, C.; Baerends, J.; Vernooijs, P. *Inorg. Chem.* **1994**, *33*, 3538.

(18) Casida, M. Time Dependent Density Functional Response Theory for Molecules. In *Recent Advances in Density Functional Methods*; Chong, D. P., Ed.; World Scientific: Singapore, 1995; Vol.1, p 155.

(19) Gross, E. U. K.; Dobson, J. F.; Petersilka, M. In *Density Functional Theory*; Nalewajski, R. F., Ed.; Springer Series Topics in Current Chemistry; Springer: Heidelberg, 1996.

(20) (a) van Gisbergen, S. J. A.; Groeneveld, J. A.; Rosa, A.; Snijders, J.; Baerends, E. J. *J. Phys. Chem. A* **1999**, *103*, 6835. (b) Rosa, A.; Baerends, E. J.; van Gisbergen, S. J. A.; van Lenthe, E.; Groeneveld, J. A.; Snijders, J. G. *J. Am. Chem. Soc.* **1999**, *121*, 10 356. (c) Ricciardi, G.; Rosa, A.; van Gisbergen, S. J. A.; Baerends, E. J. *J. Phys. Chem. A* **2000**, *104*, 635. (d) Adamo, C.; Barone, V. *Theor. Chem. Acc.* **2000**, *105*, 169. (e) Rosa, A.; Ricciardi, G.; Baerends, E. J.; van Gisbergen, S. J. A. *J. Phys. Chem. A* **2001**, *105*, 3311. (f) Ricciardi, G.; Rosa, A.; Baerends, E. J. *J. Phys. Chem. A* **2001**, *105*, 5242.

(21) Gorelesky, S. I.; da Silva, S. C.; Lever, A. B. P.; Franco, D. W. *Inorg. Chimica Acta* **2000**, *300–302*, 698.

(22) Boulet, P.; Chermette, H.; Daul, C.; Gilardoni, F.; Rogemond, F.; Weber, J.; Zuber, G. *J. Phys. Chem. A* **2001**, *105*, 885.

(23) Barone, V.; Fabrizi de Biani, F.; Ruiz, E.; Sieklucka, B. *J. Am. Chem. Soc.* **2001**, *123*, 10 742.

(24) Baerends, E. J.; Ellis, D. E.; Ros, P. *Chem Phys.* **1973**, *2*, 42.

(25) te Velde, G.; Baerends, E. J. *J. Comput. Phys.* **1992**, *99*, 84.

(26) Fonseca Guerra, C.; Visser, O.; Snijders, J. G.; te Velde, G.; Baerends, E. J. Parallelisation of the Amsterdam Density Functional Program. In *Methods and Techniques for Computational Chemistry*; Clementi, E., Corongiu, G., Eds.; STEF: Cagliari, 1995; p 305.

(27) (a) van Gisbergen, S. J. A.; Snijders, J. G.; Baerends, E. J. *J. Chem. Phys.* **1995**, *103*, 9347. (b) van Gisbergen, S. J. A.; Snijders, J. G.; Baerends, E. J. *J. Comput. Phys. Commun.* **1999**, *118*, 119.

(28) Vosko, S. H.; Wilk, L.; Nusair, M. *Can. J. Phys.* **1980**, *58*, 1200.

(29) Becke, A. D. *Phys. Rev.* **1988**, *A38*, 3098.

(30) (a) van Gisbergen, S. J. A.; Snijders, J. G.; Baerends, E. J. *J. Chem. Phys.* **1995**, *103*, 9347. (b) van Gisbergen, S. J. A.; Snijders, J. G.; Baerends, E. J. *J. Comput. Phys. Commun.* **1999**, *118*, 119. Perdew, J. P.; Wang, Y. *Phys. Rev.* **1992**, *B45*, 13 244.

(31) van Leeuwen, R.; Baerends, E. J. *Phys. Rev. A* **1994**, *49*, 2421.

(32) ADF. STO's basis set database available on line at <http://tc.chem.vu.nl/SCM/Doc/atomicdatabase>.

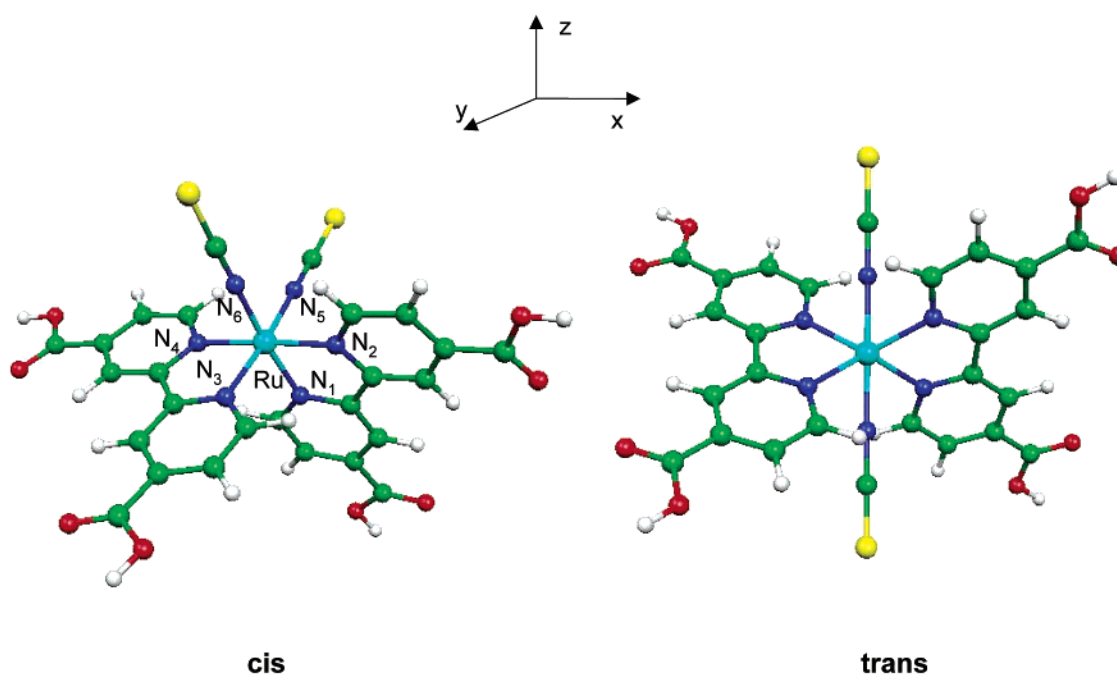


**Figure 1.** Optimized structure of the cis and trans isomers of the [Ru(4,4'-COOH-2,2'-bpy)<sub>2</sub>(NCS)<sub>2</sub>] complex.

S atoms, and one 2p for H atom. The cores (1s for C and O; 1s–2p for S; 1s–3d for Ru) were kept frozen. Hereafter, we will refer to this basis set as **BS1**. To check the convergence of our calculations with basis set expansion, TD-DFT calculations have been also performed using the ADF IV basis set<sup>32</sup> for all atoms except hydrogen, for which the ADF III basis set has been used. The ADF IV basis set for C, N, and S is an uncontracted triple-STO basis set with a polarization function. We will refer to this basis set as **BS2**.

In the calculation of the optical spectra, the 70 lowest spin-allowed singlet–singlet transitions, up to an energy of  $\sim 4.0$  eV, were taken into account. Transition energies and oscillator strengths have been interpolated by a Gaussian convolution with a  $\sigma$  of 0.2 eV.

Solvation effects were modeled by the “Conductor-like Screening Model” (COSMO)<sup>33</sup> of solvation as implemented in the ADF code,<sup>34</sup> using the structures optimized in vacuo. This solvation model differs from the “Polarizable Continuum Model” (PCM)<sup>35</sup> used in ref 23 essentially in the definition of the solute cavity and electrostatic properties of the solvent, which is treated as a conductor in COSMO and as a dielectric in PCM. Moreover, in the present ADF implementation, the solvent response to the time dependent perturbation is neglected.

### III. [Ru(4,4'-COOH-2,2'-bpy)<sub>2</sub>(NCS)<sub>2</sub>] Complex in Vacuo

**A. Molecular Structure.** In all the calculations reported in this paper, we considered the four carboxylic groups of [Ru(4,4'-COOH-2,2'-bpy)<sub>2</sub>(NCS)<sub>2</sub>] to be protonated, which represents a realistic model of the investigated complex in water solutions at pH < 1.5.<sup>9</sup> The geometry of the N3 complex with a cis arrangement of the thiocyanate ligands was optimized imposing a pseudo-octahedral  $C_2$  symmetry. The z axis is oriented along the line bisecting the  $\angle$ NRuN angle formed by the nitrogen atoms of the thiocyanate groups (see Figure 1). In Table 1 optimized geometrical parameters of N3 are compared

**Table 1.** Optimized Geometrical Parameters (bond lengths in Å and Angles in Degrees) of Complex *cis*-[Ru(4,4'-COOH-2,2'-bpy)<sub>2</sub>(NCS)<sub>2</sub>] Compared with X-ray Data (second column)

parameters	expt.	(C <sub>2</sub> )	(C <sub>i</sub> )
R <sub>Ru–N<sub>1,3</sub></sub>	2.036(15) 2.058(12)	2.079	2.078 2.083
R <sub>Ru–N<sub>2,4</sub></sub>	2.030(13) 2.013(14)	2.056	2.060 2.055
R <sub>Ru–N<sub>5,6</sub></sub>	2.048(12) 2.046(16)	2.036	2.028 2.018
$\angle$ N <sub>1</sub> RuN <sub>2</sub>	79.8(5) 79.1(5)	78.9	78.4 78.8
$\angle$ N <sub>1</sub> RuN <sub>3</sub>	90.6(5)	95.1	94.7
$\angle$ N <sub>1</sub> RuN <sub>4</sub>	97.8(5)	94.0	94.9
	95.9(5)		94.2
$\angle$ N <sub>2</sub> RuN <sub>4</sub>	174.5(6)	169.5	170.0
$\angle$ N <sub>5</sub> RuN <sub>6</sub>		90.2	89.7

Results obtained with and without  $C_2$  symmetry constraints are reported in the third and fourth column, respectively.

to available experimental data.<sup>7</sup> The agreement between computed and experimental parameters is very good: the critical ruthenium–nitrogen bonds are accurately reproduced, as well as the lengthening of the Ru–N bipyridine bonds trans to thiocyanate ligands. Moreover, our optimized structure shows a skewing of 8° of the terminal carboxylic groups with respect to the aryl moiety plane, which is again in agreement with available X-ray data.<sup>7</sup> To check the adequacy of the  $C_2$  symmetry we re-optimized the geometry of N3 without any symmetry constraints. The results, also reported in Table 1, show little deviation from the ideal  $C_2$  symmetry, which was therefore maintained throughout the paper.

We also optimized the geometry of the trans isomer of the N3 complex within  $D_2$  symmetry constraints (see Figure 1), and found it 17.5 kcal mol<sup>−1</sup> higher in energy than the corresponding cis isomer. The higher thermodynamic stability of the cis isomer is consistent with the experimental evidence that this isomer is the only product obtained by direct synthesis and that no cis–

(33) (a) Klamt, A.; Schüürmann, G. *J. Chem. Soc., Perkin Trans. 2* **1993**, 799.

(b) Klamt, A.; Jonas, V. *J. Chem. Phys.* **1996**, *105*, 9972.

(34) Pye, C. C.; Ziegler, T. *Theor. Chem. Acc.* **1999**, *101*, 396.

(35) (a) Miertuš, S.; Scrocco, E.; Tomasi, J. *Chem. Phys.* **1981**, *55*, 117. (b) Cossi, M.; Barone, V.; Cammi, R.; Tomasi, J. *Chem. Phys. Lett.* **1996**, *255*, 327.

**Table 2.** Energies and Percentage Composition of the Lowest Unoccupied and Highest Occupied Kohn–Sham Orbitals of the Complex *cis*-[Ru(4,4'-COOH-2,2'-bpy)<sub>2</sub>(NCS)<sub>2</sub>] in Terms of Ru, Dcbpy, and NCS Fragments<sup>a</sup>

MO	occ	E(eV)	Ru	dcbpy	NCS
60a	0	-3.14		90(C); 4(O)	
59b	0	-3.28		92(C)	
59a	0	-3.51	5(d <sub>z<sup>2</sup></sub> )	61(C); 15(N); 13(O)	
58b	0	-3.53	3(d <sub>yz</sub> )	65(C); 15(N); 16(O)	
58a	0	-3.92	7(d <sub>z<sup>2</sup></sub> ); 1(d <sub>x<sup>2</sup>-y<sup>2</sup></sub> ); 1(d <sub>xy</sub> )	48(C); 22(N); 5(O)	
<b>57b</b>	0	-4.08	7(d <sub>yz</sub> )	53(C); 24(N); 7(O)	
<b>57a</b>	2	-4.58	11(d <sub>xy</sub> ); 7(d <sub>z<sup>2</sup></sub> )		52(S); 19(N)
56b	2	-4.71	12(d <sub>yz</sub> )		57(S); 19(N)
56a	2	-4.72	3(d <sub>xy</sub> ); 2(d <sub>z<sup>2</sup></sub> ); 2(d <sub>x<sup>2</sup>-y<sup>2</sup></sub> )		58(S); 21(N)
55b	2	-4.84			70(S); 25(N)
55a	2	-6.08	46(d <sub>xy</sub> ); 12(d <sub>z<sup>2</sup></sub> )		20(S); 10(C)
54b	2	-6.12	55(d <sub>yz</sub> )		17(S); 15(C)
54a	2	-6.28	26(d <sub>z<sup>2</sup></sub> ); 17(d <sub>x<sup>2</sup>-y<sup>2</sup></sub> ); 9(d <sub>xy</sub> )		16(S); 20(C)

<sup>a</sup> Bold characters are used for the HOMO (**57a**) and the LUMO (**57b**).

trans isomerization is observed.<sup>8,10</sup> We therefore focused our investigation mainly on the more stable *cis* isomer.

**B. Electronic Structure.** In the *cis*-N3 complex, the Ru(II) center, characterized by a d<sup>6</sup> electron configuration, is surrounded by three inequivalent pairs of nitrogen atoms. A detailed analysis of the highest occupied and lowest unoccupied molecular orbitals of this complex is presented in Table 2, where orbital energies and composition in terms of atomic contributions are reported. The HOMO (**57a**), HOMO-1 (**56b**), and HOMO-2 (**56a**) are a set of quasi degenerate orbitals. The largest orbital contributions arise from the highest occupied thiocyanate orbitals, resulting from the combination of the sulfur *p* orbitals and nitrogen lone pairs, which mix, in an antibonding fashion, with small percentages of t<sub>2g</sub> metal orbitals, ranging from 18% to 7%. The HOMO-3 (**55b**) orbital, ~0.25 eV lower than **57a**, is localized on the thiocyanate ligands, and corresponds to a non bonding combination of a sulfur lone pair and a nitrogen *p* orbital. At lower energy (~1.6 eV with respect to the HOMO) another set of three quasi degenerate orbitals is found. These orbitals (**55a**, **54b**, and **54a**) show a predominant Ru-*d* character (58%, 55%, and 52%, respectively) and correspond to the bonding counterpart of **57a**, **56b**, and **56a**. In particular a contribution of the filled thiocyanate π orbitals combines with the t<sub>2g</sub> metal orbitals. The six lowest LUMOs (**57b**, **58a**, **58b**, **59a**, **59b**, and **60a**), lying 0.50 eV above **57a** in a range of 1.0 eV, result from the antibonding combination of the carbon and nitrogen *p* orbitals of the bipyridines with sizable contributions from the carboxylic groups. Because in photovoltaic solar cells the acidic carboxylic units serve as anchoring groups to the TiO<sub>2</sub> semiconductor surface, such a contribution from the carboxylic groups to the π\* LUMOs, which represent the final states in MLCT transitions, (see below), should favor the electron injection process from the dye excited state to the semiconductor surface.<sup>1</sup> This is due to the electron-withdrawing character of the terminal COOH groups in para position which lowers the energy of the π\* LUMOs, thus increasing the coupling between the donor energy level of the excited dye and the acceptor TiO<sub>2</sub> conduction band.

The electronic structure of the trans isomer of the N3 complex shows a group of seven highest occupied molecular orbitals, lying in a range of 1.72 eV, which result from the combination of the ruthenium t<sub>2g</sub> orbitals and thiocyanate orbitals with variable metal contributions. The six lowest LUMOs are again the bipyridine π\* orbitals, lying in a range of 1.12 eV; the

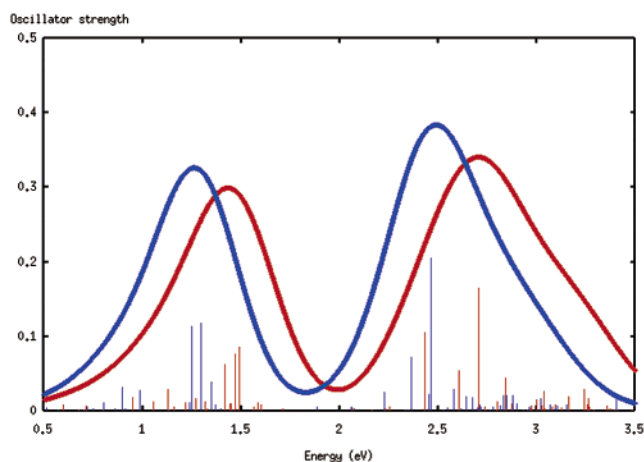


**Figure 2.** Spectrum of *cis*-[Ru(4,4'-COOH-2,2'-bpy)<sub>2</sub>(NCS)<sub>2</sub>] complex, computed in vacuo with the BPW91 (red lines) and LB94 (blue lines) XC functionals. Red (blue) vertical lines correspond to the unbroadened excitation energies and oscillator strength computed with the BPW91 (LB94) functional.

HOMO–LUMO gap is now computed to be 0.32 eV, i.e., 0.18 eV smaller than the corresponding value computed for the *cis* isomer. Interestingly, this value nicely compares with the experimental red shift of 0.17 eV observed for the first visible absorption band of the N3 complex in DMF upon *cis* to *trans* isomerization.<sup>8,10</sup> Because the LUMO energy is almost constant in the *cis* and *trans* isomers (−4.08 and −4.07 eV, respectively), the reduction of the HOMO–LUMO gap is due to raising of the HOMO energy computed in the *trans* with respect to the *cis* isomer (−4.39 vs. −4.58 eV), and can be related to the increased antibonding interactions between the metal t<sub>2g</sub> and π thiocyanate orbitals in the *trans* isomer. Such an enhanced red response of the *trans* isomer has rendered it an attractive candidate as charge-transfer sensitizer in mesoporous oxide solar cells.<sup>10</sup>

**C. Optical Absorption Spectrum.** In Figure 2, the absorption spectra of *cis*-N3 obtained using **BS2** and the BPW91 and LB94 XC functionals in the SCF step are compared. Within the investigated energy range, two well separated bands are found, with intensity maxima at 1.43 (1.26) and 2.70 (2.50) eV with BPW91 (LB94). The band line shapes, including the relative height of the two peaks, are well described by both functionals, whereas the separation of the two bands, ~1.3 eV in both cases, is significantly larger than the experimental value of ~0.8 eV. Thus, the agreement with the experiment is rather limited. Although, on the basis of these results, it is difficult to argue in favor of one functional over the other, in the following we shall use the BPW91 functional, which seems to provide a slightly better overall description of the spectrum at a lower computational cost in the SCF step. Moreover, a comparison of the spectra obtained with **BS1** and **BS2** (see the Supporting Information section, Figure S1) shows that our calculations are reasonably converged with respect to basis set expansion, with a blue-shift of only ~0.04 eV of all transition energies upon increasing the basis set from **BS1** to **BS2**; nevertheless, we adopted **BS2** throughout the paper.

BPW91-ALDA excitation energies and oscillator strengths for the first two absorption bands are reported in Tables 3 and 4, together with the composition of the solution vectors in terms of the most relevant transitions. The first absorption band has

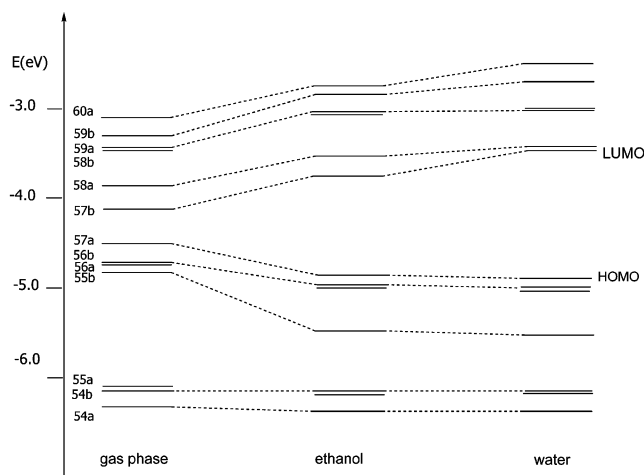
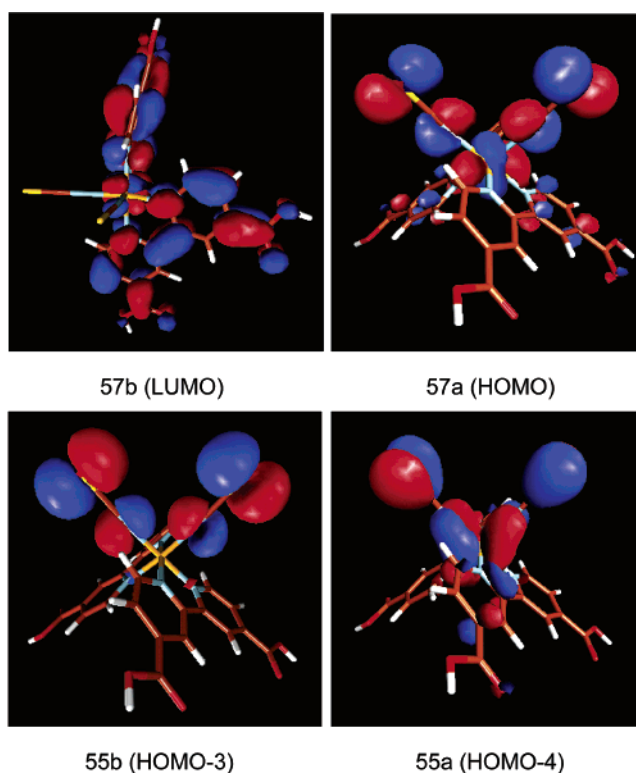
**Table 3.** Computed Excitation Energies (eV) and Oscillator Strengths (*f*) for the optical transitions with *f* > 0.01 of the First Absorption Band of N3 Complex in the Gas Phase

state	composition	<i>E</i> (eV)	<i>f</i>
3 <sup>1</sup> B	58% (56b → 58a); 15% (57a → 58b); 12% (56a → 57b); 10% (55b → 58a)	0.949	0.018
4 <sup>1</sup> B	76% (55b → 58a); 9% (56b → 58a); 6% (55b → 59a)	1.053	0.012
5 <sup>1</sup> B	79% (57a → 58b); 10% (56b → 58a)	1.128	0.028
6 <sup>1</sup> B	63% (56b → 59a); 27% (56a → 58b)	1.217	0.011
7 <sup>1</sup> B	36% (56a → 58b); 28% (57a → 59b); 22% (56b → 59a); 12% (55b → 59a)	1.273	0.016
8 <sup>1</sup> B	71% (57a → 59b); 10% (56a → 58b); 9% (56b → 59a)	1.318	0.012
8 <sup>1</sup> A	42% (57a → 60a); 15% (57a → 59a); 10% (56a → 58); 8% (56b → 58b); 8% (56a → 59a); 6% (56b → 59b)	1.415	0.062
10 <sup>1</sup> B	58% (55b → 59a); 14% (56a → 58b); 11% (56b → 59a)	1.470	0.076
10 <sup>1</sup> A	55% (57a → 60a); 13% (57a → 59a); 6% (56a → 58a)	1.489	0.086
11 <sup>1</sup> B	97% (56b60a)	1.585	0.010

**Table 4.** Computed Excitation Energies (eV) and Oscillator Strengths (*f*) for the Optical Transitions with *f* > 0.01 of the Second Absorption Band of N3 Complex in the Gas Phase

state	composition	<i>E</i> (eV)	<i>f</i>
15 <sup>1</sup> B	39% (54a → 57b); 34% (54b → 58a); 23% (55a → 58b)	2.432	0.105
16 <sup>1</sup> B	46% (55a → 58b); 41% (54b → 59a); 6% (54a → 57b)	2.605	0.054
17 <sup>1</sup> B	51% (54b → 59a); 28% (55a → 58b)	2.708	0.165
19 <sup>1</sup> B	48% (54a → 58b); 44% (55a → 59b)	2.798	0.011
21 <sup>1</sup> B	36% (54a → 58b); 34% (55a → 59b); 11% (55b → 61a); 7% (57a → 60b)	2.842	0.044
24 <sup>1</sup> B	63% (54a → 60b); 31% (54a → 59b)	2.999	0.014
26 <sup>1</sup> B	65% (54a → 59b); 30% (54a → 59b)	3.036	0.026
29 <sup>1</sup> B	93% (56a → 61b)	3.165	0.019
28 <sup>1</sup> A	32% (54a → 60a); 30% (53b → 57b); 15% (53 → 58a); 10% (55b → 61b)	3.241	0.029
29 <sup>1</sup> A	50% (55b → 61b); 26% (53b → 57b); 7% (53a → 58a); 6% (52b → 57b)	3.262	0.015

a multitransition character and involves excitations from the highest occupied to the lowest unoccupied molecular orbitals. In particular the initial states are the 55b (HOMO-3), 56a (HOMO-2), 56b (HOMO-1) and 57a (HOMO) orbitals, which have small contributions of metal *d* orbitals; the second absorption band, with onset at ~2.0 eV, involves multitransitions from the second set of HOMOs (orbitals 54a, 54b, and 55a) to the set of lowest unoccupied π\* orbitals localized on the dcby ligands. The mixed thiocyanate-metal to ligand character of both absorption bands is consistent with the electronic structure analysis discussed above, showing that the highest occupied orbitals are largely localized onto the thiocyanate ligands, in agreement with the results of previous semiempirical calculations<sup>1,14</sup> as well as with photoelectron spectroscopy<sup>14</sup> and electrochemical studies.<sup>15</sup> On the other hand, for the tetra-deprotonated [Ru(4,4'-COO-2,2'-bpy)<sub>2</sub>(NCS)<sub>2</sub>]<sup>4-</sup> complex in gas phase a quite different electronic structure has been reported,<sup>16</sup> showing two mainly Ru-based HOMOs followed by a set of five lower-lying frontier orbitals mainly localized on the anionic carboxylate groups, so that the first two UV-vis absorption bands were attributed to comparable contributions of metal and carboxylate to bipyridine charge-transfer transitions.<sup>16</sup>

**Figure 3.** Energy levels (eV) of the *cis*-[Ru(4,4'-COOH-2,2'-bpy)<sub>2</sub>(NCS)<sub>2</sub>] complex in gas phase, ethanol and water.**Figure 4.** Isodensity surface plot (isodensity contour = 0.04) of the 57b (LUMO), 57a (HOMO), 55b (HOMO-3) and 55a (HOMO-4) orbitals of *cis*-[Ru(4,4'-COOH-2,2'-bpy)<sub>2</sub>(NCS)<sub>2</sub>] complex.

#### IV. Electronic Structure in Solution and Solvatochromism

A comparison of the molecular orbital energies of the N3 complex in vacuo, ethanol and water, is shown in Figure 3, while isodensity surface plots of selected orbitals in ethanol are presented in Figure 4. Inclusion of solvation effects leads to a sizable change of both energies and composition of the molecular orbitals. In ethanol, the lowest LUMOs (orbitals 57b-60a) are significantly destabilized, by ~0.3–0.4 eV with respect to the corresponding values computed in vacuo, even though they maintain a similar composition in terms of bipyridine and carboxylic group contributions. On the other hand, the first set of HOMOs (orbitals 57a, 56b, and 56a) is stabilized by ~0.3–

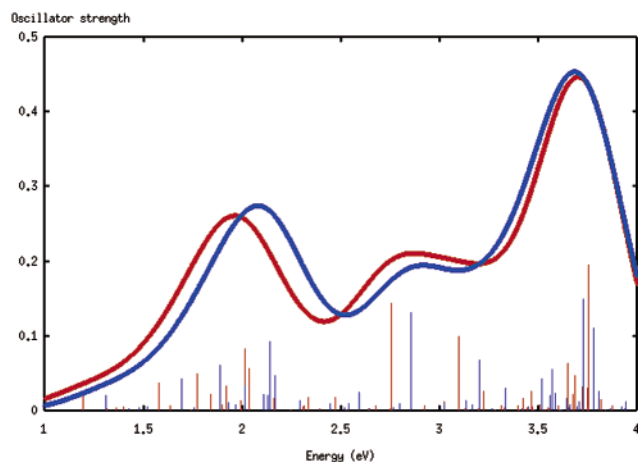


**Figure 5.** Spectra of *cis*-[Ru(4,4'-COOH-2,2'-bpy)<sub>2</sub>(NCS)<sub>2</sub>] complex computed in ethanol (red lines) and water (blue lines). Red (blue) vertical lines correspond to the unbroader excitation energies and oscillator strength in ethanol (water).

0.4 eV with respect to the corresponding values computed in vacuo, and also shows a higher contribution of ruthenium *d* orbitals mixed with NCS ligand orbitals. Orbital 55b, almost entirely localized on the thiocyanate ligands, is stabilized by ~0.6 eV. The second set of HOMOs (54a, 54b, and 55a) lies at similar energies as in the gas phase, being stabilized by 0.06 eV only, but have a somewhat different composition in terms of atomic orbitals, with slightly smaller percentages of metal states. This thiocyanate contribution to the HOMOs which are involved as starting states in the observed absorption bands (see below) is believed to have an important role in the regeneration of dye sensitized TiO<sub>2</sub> solar cells.<sup>1</sup> Altogether, the presence of the solvent leads to an important increase of the HOMO–LUMO gap, which changes from 0.50 eV in the gas-phase to 1.12 eV in ethanol.

The electronic structure of the N3 complex in water is qualitatively similar to that found in ethanol. The LUMOs 57b–60a are further destabilized, resulting in a HOMO–LUMO gap of 1.24 eV, i.e., 0.12 eV higher than that computed in ethanol. For what concerns the composition of the molecular orbitals, the main difference with respect to the gas-phase is that the ruthenium contribution in the first set of HOMOs (56a, 56b, 57a) increases up to a maximum of 40 (45)% for 57a in ethanol (water), whereas the contribution of thiocyanate orbitals is reduced to 46–58 (42–50)% within the same set. For the second set of HOMOs (54a, 54b, 55a), the metal percentages are in the range 40–33 (38–33)%, so that the metal contribution is almost the same in the two sets of HOMOs. On overall, a large electronic rearrangement appears to take place in solution, as indicated by the strong increase of the dipole moment, for which we obtain values of 19.81 and 20.60 D in ethanol and water, respectively, against a value of 10.93 D in the gas-phase, reflecting the more effective charge-separation favored by polar solvents.

The calculated optical spectra for the N3 complex in ethanol and water are shown in Figure 5. With the inclusion of 70 excitation energies, these spectra now exhibit three bands, the third band, centered at ~3.7 eV, corresponding to intraligand ( $\pi \rightarrow \pi^*$ ) multitransitions localized on the dcby ligands. The composition of the transitions in ethanol and water is rather similar, see Tables 1–3 and 4–6 of the “Supporting Informa-

**Table 5.** Energies of the Absorption Maxima, Intensities Ratio between the Maxima (in parentheses), Band Separations  $\Delta E(I-II)$  and  $\Delta E(II-III)$ , and Ethanol–Water Solvatochromic Shifts,  $\Delta E_{C_2H_5OH-H_2O}$ , for Water at pH = 1,<sup>6,9</sup> Compared to the Corresponding Calculated Values<sup>a</sup>

	expt.			$\Delta E(I-II)$	$\Delta E(II-III)$
	C <sub>2</sub> H <sub>5</sub> OH	2.30 (1.0)	3.12 (1.0)	3.95 (3.8)	0.82
H <sub>2</sub> O <sup>a</sup> (pH = 1)	2.38(1.0)	3.18(1.0)	3.97 (–)	0.80	0.79
$\Delta E_{C_2H_5OH-H_2O}$	0.08	0.06	0.02		
	ALDA/BPW91			$\Delta E(I-II)$	$\Delta E(II-III)$
	C <sub>2</sub> H <sub>5</sub> OH	1.97 (1.2)	2.86 (1.0)	3.70 (2.1)	0.89
H <sub>2</sub> O	2.08 (1.4)	2.92 (1.0)	3.69 (2.3)	0.84	0.77
$\Delta E_{C_2H_5OH-H_2O}$	0.11	0.06	–0.01		

<sup>a</sup> Energies in eV.

tion” section. In both solvents, the first two absorption bands have a mixed thiocyanate-metal to ligand character, whereas the third band is assigned to intraligand ( $\pi \rightarrow \pi^*$ ) transitions with small metal contributions. For the first band, the starting orbitals are the HOMO, HOMO-1, HOMO-2, and HOMO-3 (57a, 56b, 56a and 55b), whereas the second band originates from transitions starting from orbitals 54a, 54b, and 55a. As shown in Figure 5, the latter band is dominated by two main mixed ( $n \rightarrow \pi^*$ ) and ( $d \rightarrow \pi^*$ ) transitions, at 2.75 eV ( $f = 0.14$ ) and 3.10 eV ( $f = 0.10$ ) for the spectrum in ethanol, and at 2.85 eV ( $f = 0.13$ ) and 3.20 eV ( $f = 0.07$ ), for the spectrum in water.

It is evident that the spectra in Figure 5 are in considerably better agreement with the experiment than the spectrum computed in vacuo, in terms of both band positions and separations. Indeed, inclusion of solvation effects blue-shifts the first and second band by ~0.5 and ~0.2 eV in both solvents with respect to the gas phase. Absorption maxima energies, band separations and relative intensities of the three bands have been collected in Table 5, together with the solvatochromic energy shifts of water with respect to ethanol. In particular, in ethanol we find that the separation between the first and second band and that between the second and third band are 0.89 and 0.84 eV, respectively, while the corresponding experimental values are 0.82 and 0.83 eV. Similarly, in water the calculated band separations are 0.84 and 0.77 eV, to be compared to the experimental values of 0.80 and 0.79 eV. Moreover, in qualitative agreement with the trend observed experimentally, the ( $\pi \rightarrow \pi^*$ ) band is computed to be much more intense than the first (almost equally intense) two bands, by a factor of ~2. On overall the main spectral features are well reproduced by our theoretical model, even though both spectra in Figure 5 are red-shifted by ~0.3 eV with respect to the experiment. This residual red-shift is probably due to the use of the BPW91 exchange-correlation functional in the SCF step,<sup>36</sup> i.e., the BPW91 underestimate of HOMO–LUMO gaps is not fully corrected by the TD-DFT excitation energies.

An interesting difference between the spectra in ethanol and water, is the general blue-shift of the first two bands with increasing solvent polarity, which represents the signature of the negative solvatochromism shown by the N3 complex.<sup>6</sup> Experimentally, the maxima of the first two absorption bands in water (pH = 1) are shifted by 0.08 and 0.06 eV with respect to ethanol (see Table 5). In excellent agreement with these data,

(36) (a) Adamo, C.; Scuseria, G.; Barone, V. *J. Chem. Phys.* **1999**, *111*, 2889. (b) Cave, R. J.; Burke, K.; Castner, E. W., Jr. *J. Phys. Chem. A* **2002**, *106*, 9294.

the corresponding values from our calculations are 0.11 and 0.06 eV. Also in agreement with the experiment, we find that the ( $\pi \rightarrow \pi^*$ ) band is only weakly affected by the change in solvent polarity. This reflects the fact that the  $\pi \rightarrow \pi^*$  transitions give rise to an electron density redistribution within the bipyridine  $\pi$  framework.

To get insight into the origin of the negative solvatochromism of the first two absorption bands, it is useful to keep in mind the electronic structure of the complex in solution, together with the characterization of the absorption spectrum in terms of one electron excitations discussed above. Electronic excitations from the first two sets of HOMOs to the first LUMOs involve displacement of electron charge from the Ru center and the NCS ligands toward the delocalized bipyridine  $\pi^*$  orbitals. Thus, a reduction of the dipole moment in the excited state is expected, and, as a consequence, the excited state should be less stabilized by polar solvents than the ground state. To approximately evaluate the dipole moment in the excited state ( $\mu_{\text{ex}}$ ), we considered the electronic state in which one electron is promoted from the HOMO (57a) to the LUMO (57b). We found  $\mu_{\text{ex}} = 5.26$  D in the gas phase, with a reduction  $\Delta\mu = 5.67$  D with respect to the dipole moment in the ground state, and, similarly,  $\mu_{\text{ex}} = 9.56$  D with  $\Delta\mu = 10.25$  D in ethanol, and  $\mu_{\text{ex}} = 10.11$  D with  $\Delta\mu = 10.49$  D in water. The small increase of  $\Delta\mu$  with increasing solvent polarity well correlates with the observed negative solvatochromism.

## V. Summary and Conclusions

The electronic, structural and spectroscopic properties of the [Ru(4,4'-COOH-2,2'-bpy)<sub>2</sub>(NCS)<sub>2</sub>] complex (N3) in vacuo and in ethanol and water solvents have been investigated by means of combined DFT/TD-DFT calculations. The geometries of both the cis and trans isomers have been optimized, and the cis isomer was found to be 17.5 kcal mol<sup>-1</sup> more stable than the trans isomer. For the latter, the computed reduction of the HOMO–LUMO gap with respect to the cis isomer (0.18 eV) nicely compares with the experimental red shift of 0.17 eV observed for the first absorption band upon cis to trans isomerization.

Frontier orbital analysis, performed on the cis isomer in solution, shows that the first HOMOs are composed by almost equal contributions of thiocyanate *p* orbitals and ruthenium *t*<sub>2g</sub> *d* orbitals. Moreover, we find a set of quasi-degenerate LUMOs of  $\pi^*$  character, resulting from antibonding combinations of bipyridine carbon *2p* orbitals, with sizable contributions from

the carboxylic groups. These thiocyanate and carboxylic groups contributions to the HOMOs and LUMOs, respectively, are believed to have an important role in the regeneration and electron injection performance of dye sensitized TiO<sub>2</sub> solar cells.

Interestingly, the overall shape and band separations of the N3 spectrum are well reproduced only after inclusion of solvation effects, reflecting the major changes in the electronic structure observed in solution. We assign the first two bands to charge-transfer transitions to the bipyridine ligands originating from hybrid orbitals made up of comparable metal and thiocyanate contributions. The third band, almost twice as intense as the first two bands, is assigned to intraligand  $\pi \rightarrow \pi^*$  transitions. In addition, our results quantitatively reproduce the solvatochromic shifts exhibited by the N3 complex with increasing solvent polarity; we find shifts of 0.11 and 0.06 eV for the first and second absorption band, respectively, to be compared to the experimental shifts of 0.08 and 0.06 eV. This negative solvatochromism appears to be related to a decreased dipole moment in the excited state with respect to the ground state, which translates into a higher stabilization of the ground state in solvents of increasing polarity.

Finally, the results of this work show that careful DFT/TD-DFT calculations are capable of accurately describing the spectral features and solvatochromism of the N3 sensitizer, with a quantitative agreement with the experimental data. This suggests that such a theoretical approach may provide useful insight in the design of new and more efficient photosensitizers for TiO<sub>2</sub> solar cells and other devices of the same type.

**Acknowledgment.** All the calculations have been performed on the IBM-SP3 computer at ISTM-CNR (Perugia). We thank Prof. A. Sgamellotti and Dr. C. Miliani for helpful discussions. S.F. thanks the CNR (“Short-term mobility”-2001) for financial support.

**Supporting Information Available:** Spectra of [Ru(4,4'-COOH-2,2'-bpy)<sub>2</sub>(NCS)<sub>2</sub>] complex computed in vacuo with **BS1** and **BS2**. Excitation energies, oscillator strength (*f*) and composition of the BPW91/ALDA solution vectors for the spectrum of [Ru(4,4'-COOH-2,2'-bpy)<sub>2</sub>(NCS)<sub>2</sub>] in ethanol and water. This material is available free of charge via the Internet at <http://www.pubs.acs.org>.

JA0207910